Development of a low-cost point of care device for near-infrared spectroscopy (NIRS) based online imaging during non-invasive electrical brain stimulation

FINAL REPORT Submitted to

INRIA-DEMAR team

for

Summer Internship

By

Utkarsh Jindal

Graduate Student

Electronics and Communication Engineering Department

International Institute of Information Technology,

Hyderabad – 500032, INDIA

INVENTORS FOR THE DIGITAL WORLD

Object: Certificate of completion of internship

It is certified that Mr. Utkarsh Jindal, currently a student of 5th year Electronics and Communication Engineering Department, International Institute of Information Technology, Hyderabad, India has successfully completed his Summer Internship from May 15-Aug 15, 2015 at the INRIA DEMAR Team of Montpellier Laboratory of Informatics, Robotics, and Microelectronics (LIRMM in French) - a cross faculty research entity of the University of Montpellier 2 (UM2) and the National Center for Scientific Research (CNRS) - Institut des sciences informatiques et de leurs interactions (INS2I) Montpellier, France.

David Guiraud (PhD)
Scientist leader of INRIA DEMAR Team
University of Montpellier - LIRMM
860 Rue Saint Priest
F-34095 Montpellier Cedex 5
Tel: +33 467 418 621
Sec: +33 467 418 688
Web: http://www.lirmm.fr/demar
Perso: http://www.lirmm.fr/~guiraud

Acknowledgement

I wish to express my sincere thanks to **Dr. David Guiraud, Senior Research Scientist INRIA and Head Team DEMAR, LIRMM INRIA Montpellier,** for accepting me as an internee in his team, supporting me throughout the course of this internship program. I wish to express my deep gratitude to **Dr. Anirban Dutta, INRIA starting research scientist, DEMAR team** for giving me a chance to pursue such an interesting project under Franco-Indian INRIA-DST funding and for constantly guiding and supervising me in research areas which were new to me.

I am grateful to **Ms. Rand Almajidy, Research Associate**, for helping me with the phantom testing (under Franco-German PHC PROCOPE funding) at the research laboratory of **Prof. Dr. rer. nat. Ulrich G. Hofmann, Peter-Osypka-Professor for Neuroelectronic Systems, University Medical Center Freiburg, Department of Neurosurgery, Germany.**

I am grateful to **Mr. Victor Vagne, Doctoral Student**, for helping with the bench testing of SomaSensor (under CHRU Montpellier support) at the research unit of **Dr. Emmanuelle Le Bars and Dr. Nicolas Menjot de Champfleur, Plateforme d'Imagerie Fonctionnelle Humaine, Centre Hospitalier Régional Universitaire (CHRU) de Montpellier, France.**

I am very grateful to **Dr. Shubhajit Roy Chowdhury, Assistant Professor at the International Institute of Information Technology, Hyderabad, India** and a collaborator under Franco-Indian INRIA-DST funding for providing me an opportunity to travel to France and complete the project that I started in India under his guidance. The project consumed hard work, lot of research and dedication, and wouldn't have been possible without the support of all my supervisors and organizations I worked with.

My thanks and appreciations also go to my colleague, **Ms. Mehak Sood,** who willingly helped me out with her abilities throughout the project.

I attribute the completion of this research study to the blessings, moral support, love and affection of my parents and family members. They have always been a major source of motivation and strength.

Finally, I would like to express my recondite thanks to all those who have rendered their much needed services in the realization of this work.

Chapter 1: Introduction

All of us are exposed to optical (i.e., visible and near-infrared) radiation from the sun and other sources throughout our lives. Assuming our eyes are shielded from excessive intensity, and our skin is protected from the ultraviolet content of sunlight, we accept this exposure in the knowledge that it is perfectly safe. Unlike x-rays, optical photons are insufficiently energetic to produce ionisation, and unless light is concentrated to such a high degree that it causes burning to the skin, optical radiation offers no significant hazard. The diagnostic potential of optical methods has been widely known since Jöbsis [1] first demonstrated that transmittance measurements of near-infrared (NIR) radiation could be used to monitor the degree of oxygenation of certain metabolites. This led to the development and increasingly widespread use of clinical near-infrared spectroscopy (NIRS), which offers a safe, non-invasive means of monitoring cerebral function at the bedside without the use of radioisotopes or other contrast agents [2].

Human tissues contain a variety of substances whose absorption spectra at NIR wavelengths are well defined, and which are present in sufficient quantities to contribute significant attenuation to measurements of transmitted light. The concentration of some absorbers, such as water, melanin, and bilirubin, remain virtually constant with time. However, some absorbing compounds, such as oxygenated haemoglobin (HbO_2), deoxyhaemoglobin (Hb), and oxidised cytochrome oxidase (CtOx), have concentrations in tissue which are strongly linked to tissue oxygenation and metabolism. Increasingly dominant absorption by water at longer wavelengths limits spectroscopic studies to less than about 1000 nm. The lower limit on wavelength is dictated by the overwhelming absorption of Hb below about 650 nm. However, within the 650-1000 nm window, it is possible with sensitive instrumentation to detect light which has traversed up to 8 cm of tissue [3].

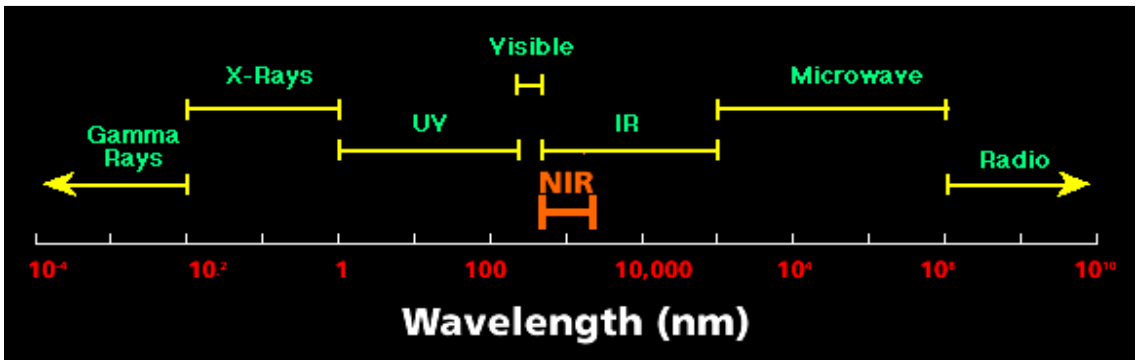

Fig 1.1. Complete spectral range

Functional near infrared spectroscopy (fNIRS) is based on the optical measurement of changes in tissue oxy-(*HbO*2), and deoxy-(*Hb*) haemoglobin concentration whereas cerebral oximetry is cerebral oxygenation monitoring via near-infrared spectroscopy (NIRS) [3]. One aspect of this response - the blood oxygen level dependent (BOLD) signal is the basis for functional magnetic resonance imaging (fMRI), a brain imaging modality closely related to fNIRS in terms of the underlying measurand. The responses measured during fNIRS are usually interpreted in terms of

changes in *HbO*2 and *Hb* concentration -- a somewhat richer set of variables than those available from basic fMRI. A third hemodynamic variable, *Hbt*, can be derived as the sum of *HbO*2 and *Hb* concentrations, which is considered a good indicator of the variations in the regional cerebral blood volume (CBV) [4].

NIR wavelengths can be selected such that the change in concentration of oxy-hemoglobin (HbO2) and deoxy-hemoglobin (Hb) in the brain tissue can be detected. Such a spectrophotometric determination is based on the absorption maximum of oxyhemoglobin and the isosbestic point of oxyhemoglobin and hemoglobin [5]. NIRS instrumentation works on various measuring principles, e.g., continuous wave (CW), frequency domain (FD), and time domain (TD). Absolute concentration measurements may be possible with more expensive TD and FD techniques [6] but exact quantification was not a crucial factor in our application since we only wanted to detect a relative change in HbO2 and Hb rather than to quantify the hemodynamic response in absolute terms.

Chapter 2: fNIRS System Development

Functional Near Infrared Spectroscopy is used for the purpose of neuroimaging using Near Infrared spectrum. The scalp, skull, and surrounding tissues of the brain exhibit an optical window of tissue transparency in the near-infrared (NIR) range allowing interrogatory measurements of neurochemistry at the cortex. fNIRS is a noninvasive imaging method involving the quantification of chromophore concentration resolved from the measurement of near Infrared light attenuation. Using fNIRS, brain activity is measured through hemodynamic responses associated with neuron behavior. For this, we use a source-detector pair, where the detector measures the changes in intensity of NIR light provided by the source. From the changes in detected NIR light intensities, it is possible to calculate concentrations of absorbers (termed chromophores) in the tissue such as Hb and HbO. The differences in the absorption spectra of HbO and Hb allow us to measure the relative changes in hemoglobin concentration through use of light attenuation at multiple wavelengths. The next section explains the Beer Lambert law which relates the chromophore concentration change in the tissue to the absorption of light by the chromophore.

2.1. Beer Lambert law and its application

The relationship between light intensities and chromophore concentration is commonly expressed using the Beer-Lambert law.

$$A = log\left(\frac{I}{I_o}\right)\varepsilon \cdot C \cdot d \qquad (1)$$

Attenuation (A) is the logarithmic ratio of two intensities, the intensity of the incident light (I0) and the transmitted light (I).

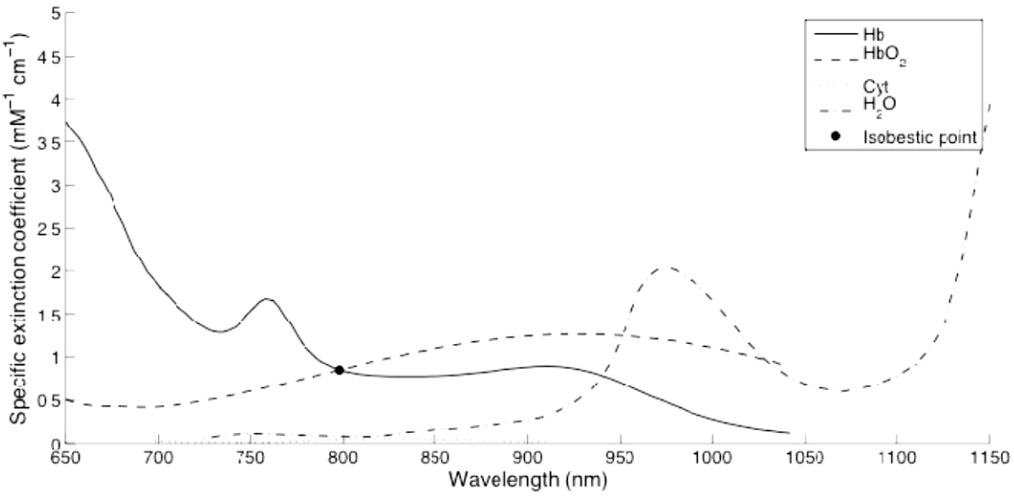

Fig 2.1. Variation of spectral extinction coefficient

ε is the molar extinction coefficient, as shown in Fig. 1, expressed in mM-1cm-1. C is the concentration of a chromophore and d is the direct path-length of the photon from the emitting to the receiving optode, i.e. the inter-optode or geometrical distance [7].

Considering that there are more chromophores in the tissue, the Beer-Lambert law can be written using that the absorption coefficient of each chromophore as additive [4], i.e.

$$A = [\varepsilon_1 \cdot C_1 + \varepsilon_2 \cdot C_2 + \ldots + \varepsilon_n \cdot C_n] \cdot d \qquad (2)$$

The typical application of the Beer-Lambert law is that A is experimentally measured (at n wavelengths for n chromophores of interest). Assuming that d is the inter-optode distance and ε1… εn has been found previously for each chromophore, the objective is to find C1…Cn [10]. Accurate estimation of chromophore concentration requires (at a minimum) the same number of wavelengths, as there is chromophores in the given tissue. A similar specific extinction coefficient of Hb and HbO2 in the near-infrared spectrum makes measuring at a single wavelength difficult and confounds the interpretation of changes in concentration of the chromophores. Simultaneous measurements of two wavelengths can be used to separate the changes for both Hb and HbO2 [8]. To increase the sensitivity of the estimation, two wavelengths should be chosen in order to distinguish between Hb and HbO2 molar extinction coefficients, such that HbO2 has the highest molar extinction coefficient at one wavelength and the lowest at the other.

However, if 'd' is not equal to the inter-optode distance, the hemoglobin changes cannot be quantified and comparisons between different subjects or NIRS regions cannot be made. d depends on subject's characteristics, the measured region, and the wavelength of the light. Due to scattering d will increase in an unknown manner. Approximately 80% of the total attenuation of near infrared light in tissue is due to scattering, and the remaining 20% to absorption [2]. Scattering is thus the biggest problem when attempting quantitative measurements with NIRS. In a highly scattering medium, photons travel a mean distance that is far greater than d, which has been defined as the differential path-length (DP), i.e., the true optical distance between the optodes. Delpy et al. [6] defined a scaling factor to correct for the path-length; the differential path-length factor (DPF). Therefore, the modified Beer-Lambert law incorporates the additions

$$A = log\left(\frac{I}{I_0}\right) = \varepsilon \cdot C \cdot d \cdot DPF + G \qquad (3)$$

The attenuation and the specific extinction coefficient in the modified Beer-Lambert law are no longer strictly linearly related, the degree of non-linearity is a function of the scattering coefficients. The scattering coefficient of the tissue together with the geometry of the optodes are described in the term G. G is unknown and therefore an absolute calculation of chromophore concentration that cannot be derived from Eq. 3. This is a fundamental problem in tissue NIRS, making the determination of absolute concentrations of Hb and HbO2 problematic. Assuming that G has the same value for all chromophores in the medium, by using a differential equation between two chromophores, G is cleared. As a consequence, only changes in concentration of chromophores can be measured with NIRS [9]. Assuming that DPF and d remain constant during

the measuring period, and d and DPF are known, quantitative data on changes in the concentration of chromophores can be derived.

$$\Delta(A) = \varepsilon \cdot \Delta(C) \cdot d \cdot DPF \quad (4)$$

The changes in the concentration of chromophores can be calculated using a different wavelength for each chromophore, writing a Beer-Lambert equation for each, and solving the simultaneous equations through matrix inversion [6]. The NIRS technique can still be applied as an oxygenation trend monitor if the DPF is unknown, such as the continuous wave NIRS. There are several techniques available that can be used to calculate the DPF, i.e., by time domain [9], frequency domain [10] or derivative spectroscopy [9], which allow for oxygenation changes to be measured. However, without the knowledge of the term G the absolute chromophore concentration cannot be measured.

2.2. Sensor implementation for continuous wave (CW) fNIRS

For hardware implementation of sensitive equipment, several factors are crucial for its performance and efficiency. As with any physiological measurement, the standardization of sensor placement, coupling, signal preprocessing, and conditioning together with a well-described experimental paradigm are essential elements in obtaining repeatable performance, optimized signal-to-noise ratio (SNR) and hence reduced workload on the DSP component. Measurement methods for NIRS are based around three distinct technologies:

- continuous wave (CW)
- frequency domain
- time domain

We are using continuous wave (CW) NIRS in this work. This method generally employ either a multiple discrete wavelength source or a filtered white light source, they measure the light attenuation using either a photomultiplier, photodiode or an avalanche photodiode detector [9]. The main advantages of CW NIRS are the sampling rate, the size of the instrument, the weight, the simplicity and the cost, which makes CW NIRS ideal for bedside monitoring. However, CW NIRS has a few disadvantages, including the penetration depth and the difficulty to separate absorption and scattering effects. CW NIRS is therefore only fit to do oxygenation trend monitoring

The basic design of our NIRS probe along with the alignment of the light emitting diode (LED) and photo-detectors are shown in Fig 2.2. S1 and S2 indicate LED and D1 and D2 are photo-detectors. The distance between the source and detector was maintained at 2.5cm. The wavelength of the source LED's are 850nm and 760 nm. The photo detector that was used is BPW34S with Dimensions (L x W x H in mm) 5.4 x 4.3 x 3.2 and Radiant sensitive area (in mm2) 7.5. The spectral bandwidth range was between 430-1100 nm. The angle of half sensitivity was 65 degrees.

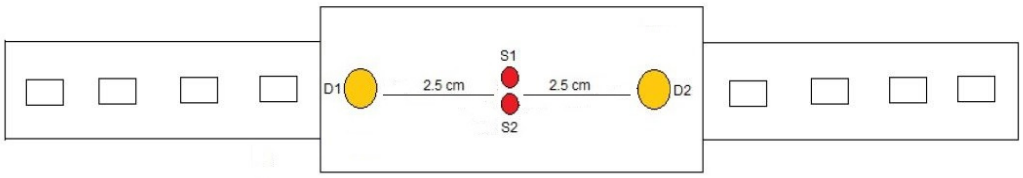

Fig 2.2. Design of custom made NIRS probe

The low-cost two channels functional NIRS hardware was implemented that captured the hemodynamic changes in the frontal cortex of the brain due to non-invasive brain stimulation as a measure of cerebrovascular reserve. The signal obtained at two channels (2 detectors) was high pass filtered (fc=0.8 Hz) (using passive high pass filter) and amplified by an instrumentation amplifier (INA131) (see Fig 2.3) followed by low pass filtering with a fourth order Butterworth low pass filter (fc=8.86 Hz) (see Fig 2.4). The INA131 is a low cost, general purpose low gain, G = 100, instrumentation amplifier offering excellent accuracy. The INA131 is laser trimmed to achieve very low offset voltage (50µV max), drift (0.25µV/°C max), and high CMR (110dB min).

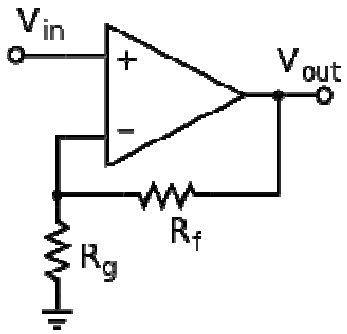

Fig 2.3. Basic design of amplifier

For implementing the Butterworth low pass filter, Texas Instrument's high precision dual operational amplifier IC OPA2277 was used. They offer improved noise, wider output voltage swing, and are twice as fast with half the quiescent current. Features include ultralow offset voltage and drift, low bias current, high common-mode rejection, and high power supply rejection. The block diagram of the setup is illustrated in Fig 2.5.

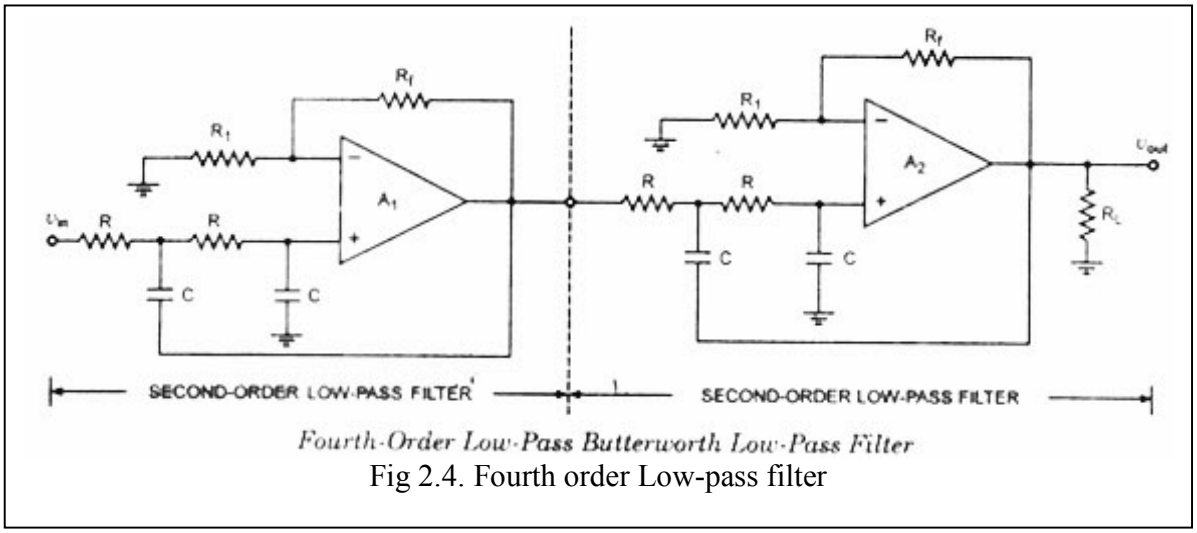

Fig 2.4. Fourth order Low-pass filter

The analog signal obtained at the output of the low pass filter was converted to digital values using the 10 bit ADC present in Arduino Uno. The digital values were ported to the computer via USB with Arduino Uno serial USART port for processing in MATLAB. The sampling rate for ADC conversion was kept at 80Hz.

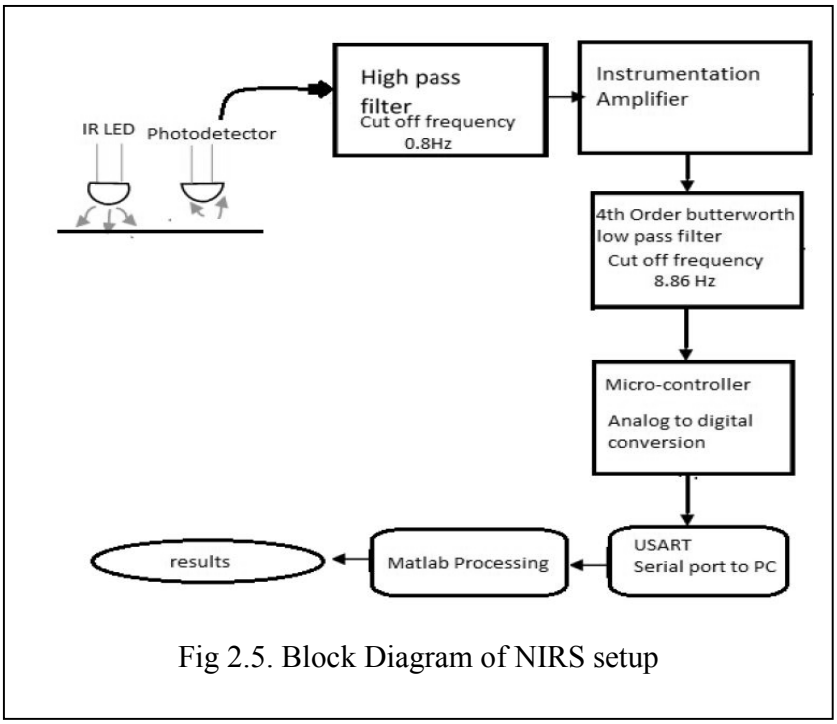

Fig 2.5. Block Diagram of NIRS setup

The Arduino was powered from USB port which was connected to the laptop. The 5V power output of the Arduino was used to power the entire circuit except the LED's. The LED's were powered using the digital output pins of the Arduino. The digital output pins of the Arduino were programmed for switching the LEDs ON/OFF systematically. The negative power (-5V) required

by OPA2277, INA131 and photodetectors was generated by using Interstil's ICL7660 CMOS voltage converter (see Fig. 2.6).

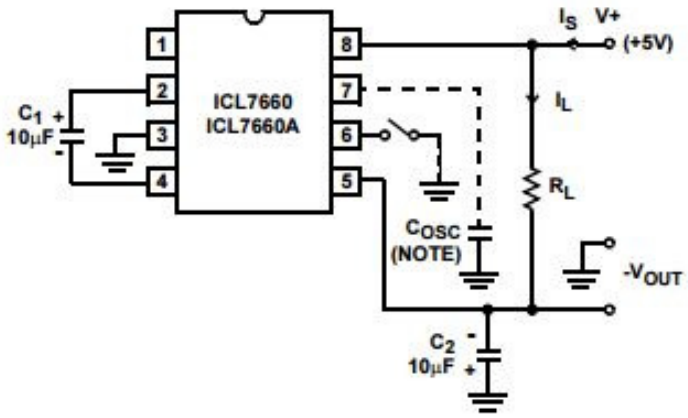

Fig 2.6. Pin connections with 7660 voltage converters

For the experimental bench-testing, the NIRS probe was placed at the F3/F4 position (10-20 international system of scalp sites) – see Fig. 2.7. NIRS data consisted of a series of time-dependent voltage signals measured between individual light source and detector positions on a probe. The concentrations of oxygenated, deoxygenated and total hemoglobin were calculated for each source-detector pair. Differential oxy hemoglobin and de-oxy hemoglobin concentrations were then estimated using modified Beer Lambert's Law with the custom software written in MATLAB (The MathWorks, Inc., USA).

The cost of the major components used in the POCT NIRS hardware are given below in Table 1

Table 1

Component	Price (USD)
OPA2277	9
INA131	10
AD129 (used later)	30
ICL7660	< 1
Arduino Uno	30
Somasensor (used later)	~300

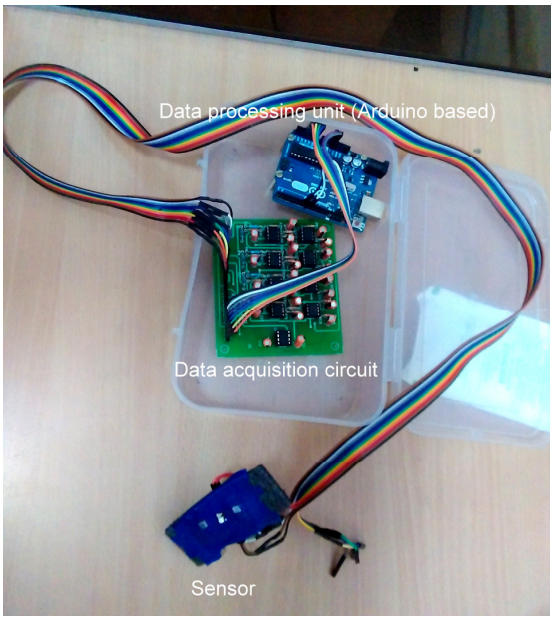

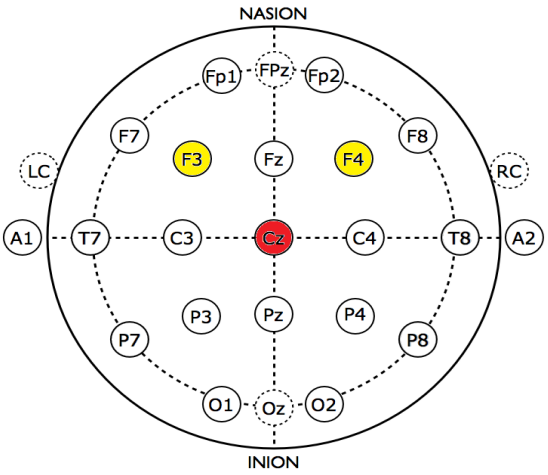

Fig 2.7. Left Panel: POCT NIRS hardware. Right Panel: 10-20 International system of scalp sites for the placement of the sensors.

Chapter 3: Bench-testing CE-approved Somasensor for clinical investigation

Clinical investigation is defined as a "Systematic investigation in one or more human subjects, undertaken to assess the safety or performance of a medical device" (ISO 14155). The low-cost NIRS sensor developed under INRIA-DST project funding needed a performance evaluation that is defined as "Investigation of an in-vitro diagnostic medical device intended to validate the performance claims under the anticipated conditions of use" (EN 13612:2002). However, the goal of the present study at INRIA, France and CHU, Montpellier was to prepare the low-cost NIRS data acquisition (DAQ) device to monitor hemodynamics during non-invasive brain stimulation (NIBS) using CE-approved SomaSensor (Covidien, USA) under a "clinical study in human subjects of a CE-marked device (being used within indication) to evaluate additional parameters." Here, Medical Devices Directive covers a diverse range of devices that are classified into one of four risk-based Classifications. Our SomaSensor based low-cost NIRS data acquisition device to monitor hemodynamics during NIBS should be classified as Class IIa - Medium risk, often short-term invasive device. These clinical tests were run with the help of Mr. Victor Vagne, Doctoral Student, at the research unit of Dr. Emmanuelle Le Bars et Dr. Nicolas Menjot de Champfleur, Plateforme d'Imagerie Fonctionnelle Humaine, Centre Hospitalier Régional Universitaire (CHRU) de Montpellier, France under CHRU Montpellier support.

Figure 3.1. SomaSensor based low-cost NIRS data acquisition device to monitor hemodynamics during NIBS.

To successfully interface the SomaSensor (Covidien, USA) with the low-cost DAQ (presented in Chapter 2), the maximum current that can go through the LED's in the SomaSensor had to be found out experimentally. This was done by varying the current through each LED in the SomaSensor and then looking at the radiant intensity changes along with the changes in the temperature of the SomaSensor. For this, we used a spectrometer Princeton Instrument SP2150 with a CCD Princeton device Pixis Excelon 400B. We also used a diffraction grating with 600

grooves/mm blazed at 500nm and the exposition time was set at 3µs. The graphs of the experiments are shown below.

Graphs of 730nm LED at different current settings: 75mA was considered the maximum and 56mA the operational current for safety as discussed in Chapter 5.

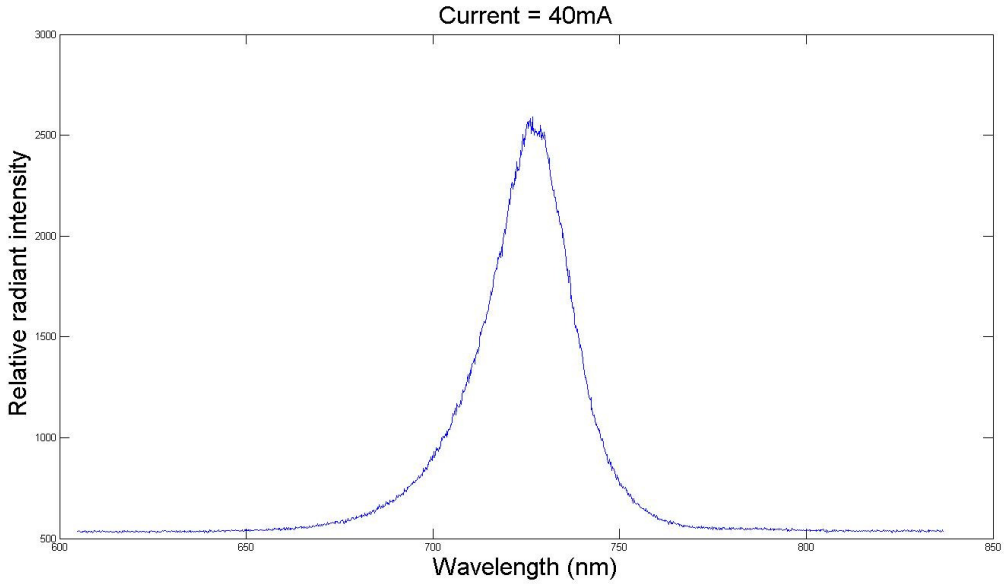

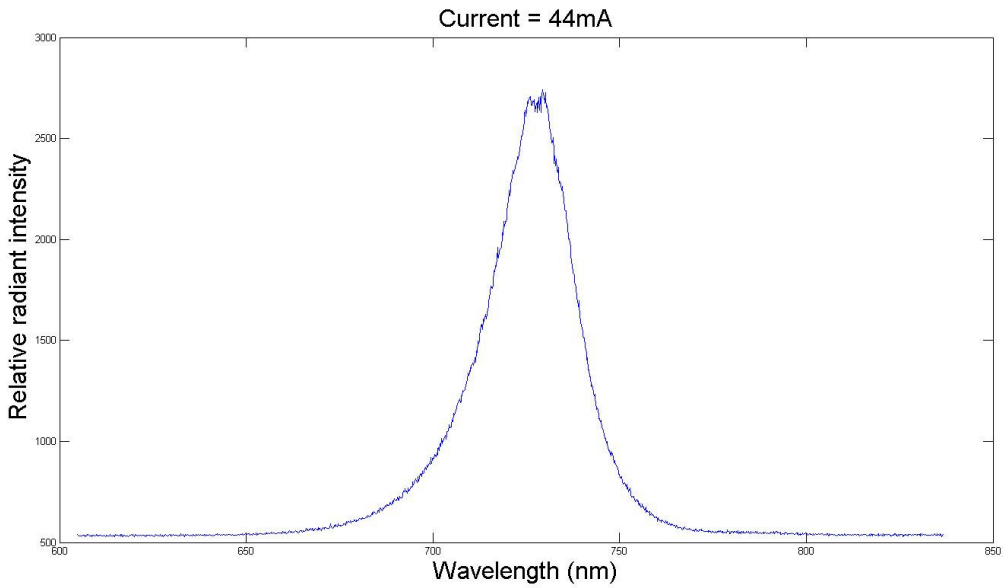

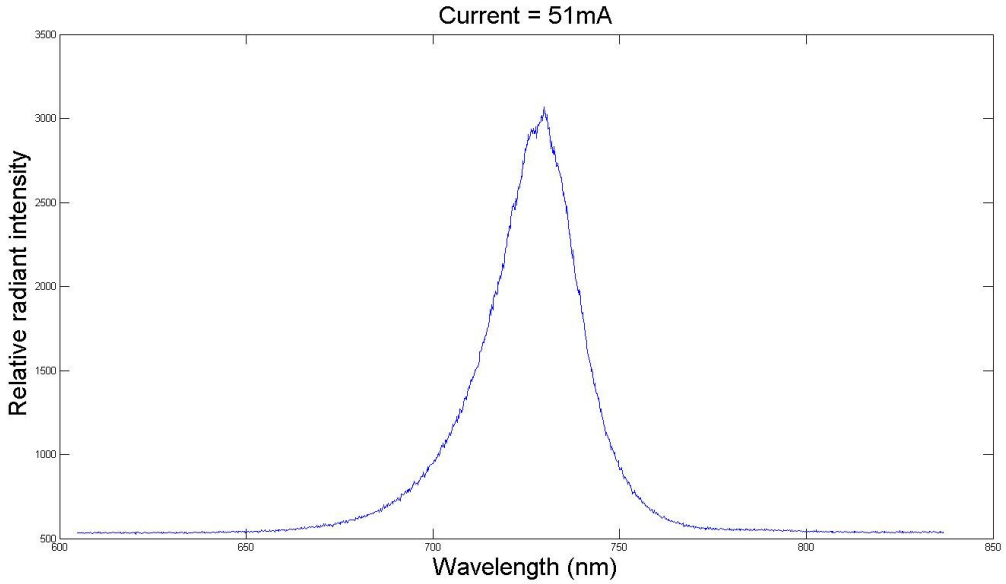
Current = 51mA
Relative radiant intensity
Wavelength (nm)
3500
3000
2500
2000
1500
1000
500
600
650
700
750
800
850

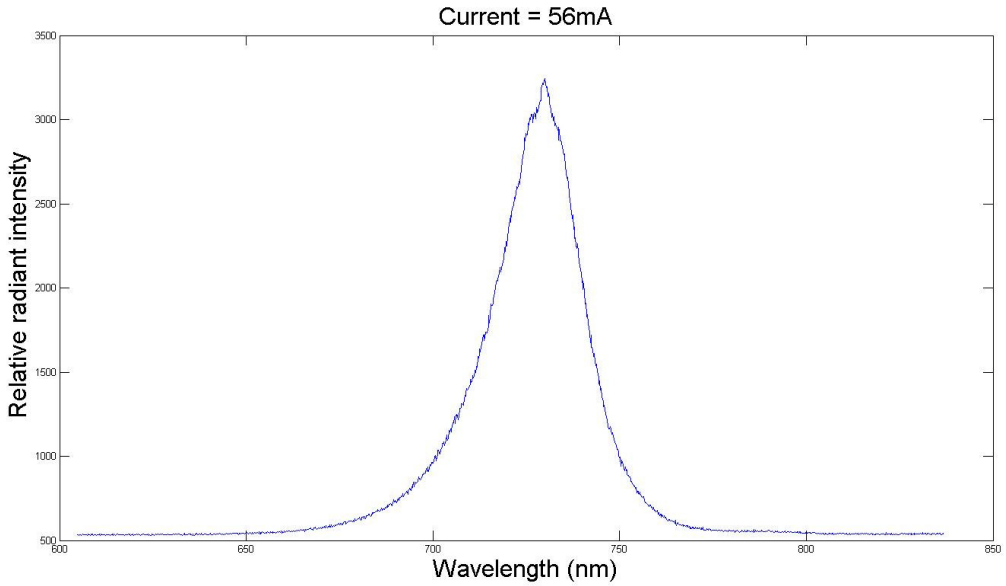
Current = 56mA
Relative radiant intensity
Wavelength (nm)
3500
3000
2500
2000
1500
1000
500
600
650
700
750
800
850

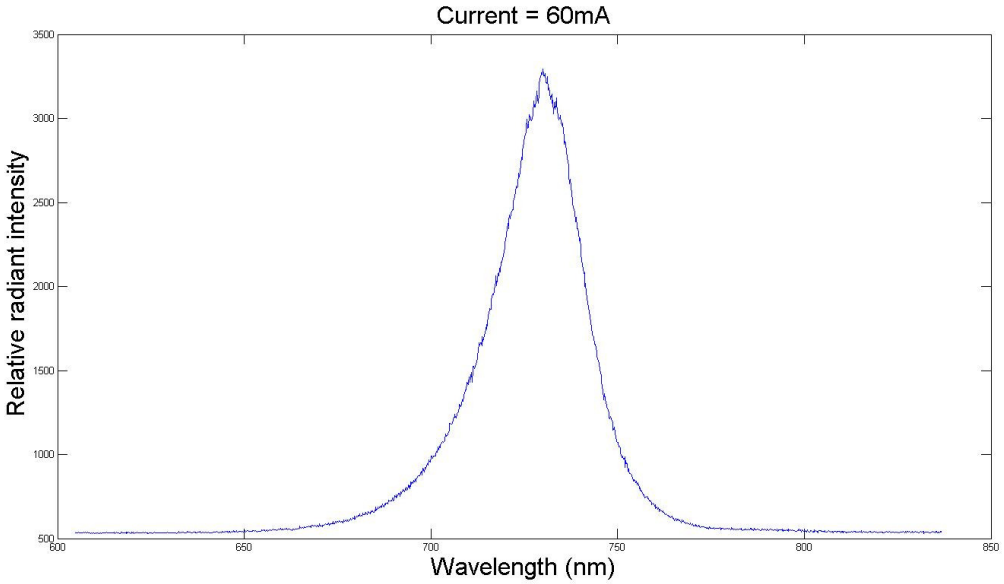
Current = 60mA
Relative radiant intensity
Wavelength (nm)
3500
3000
2500
2000
1500
1000
500
600
650
700
750
800
850

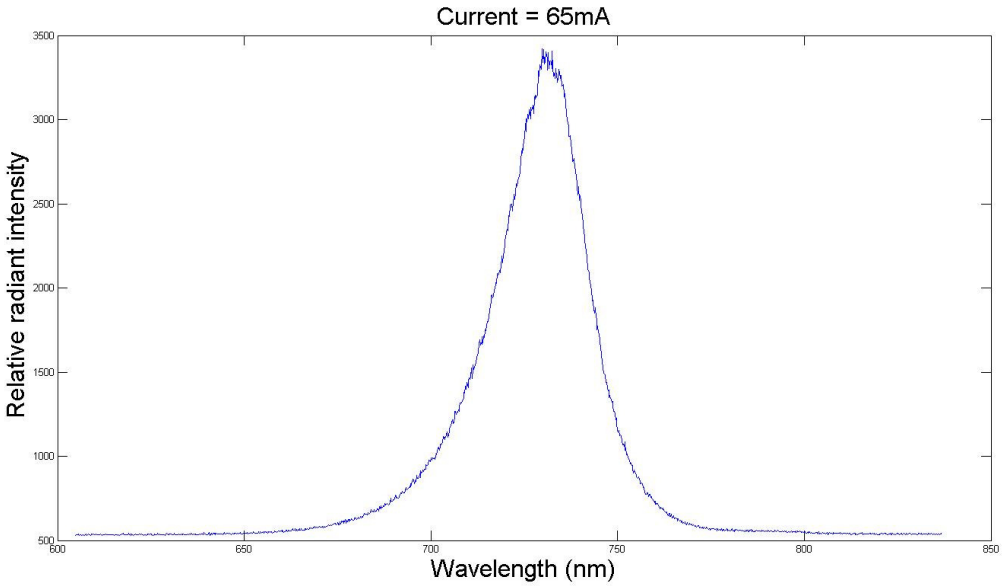
Current = 65mA
Relative radiant intensity
Wavelength (nm)
3500
3000
2500
2000
1500
1000
500
600
650
700
750
800
850

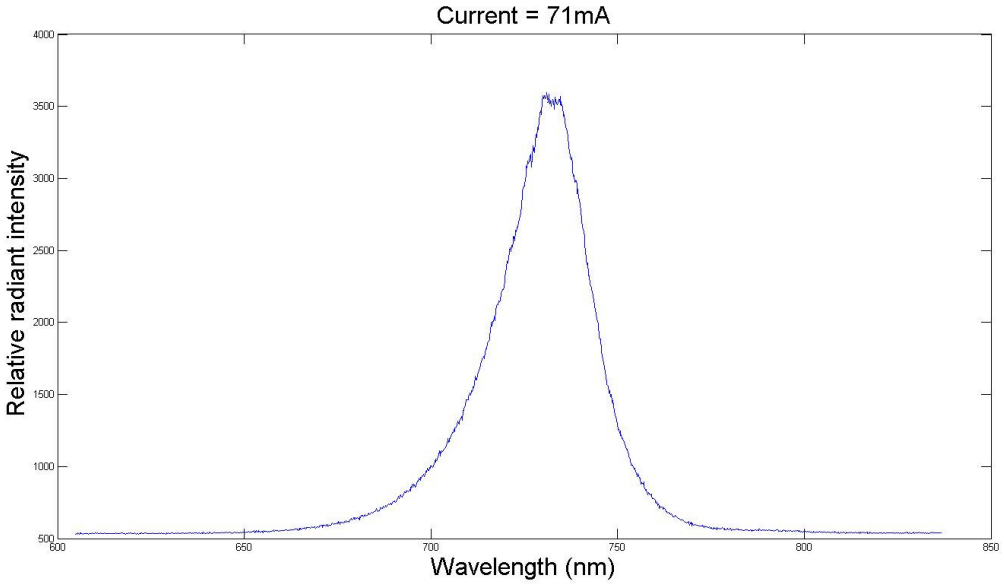
Current = 71mA
Relative radiant intensity
Wavelength (nm)
4000
3500
3000
2500
2000
1500
1000
500
600
650
700
750
800
850

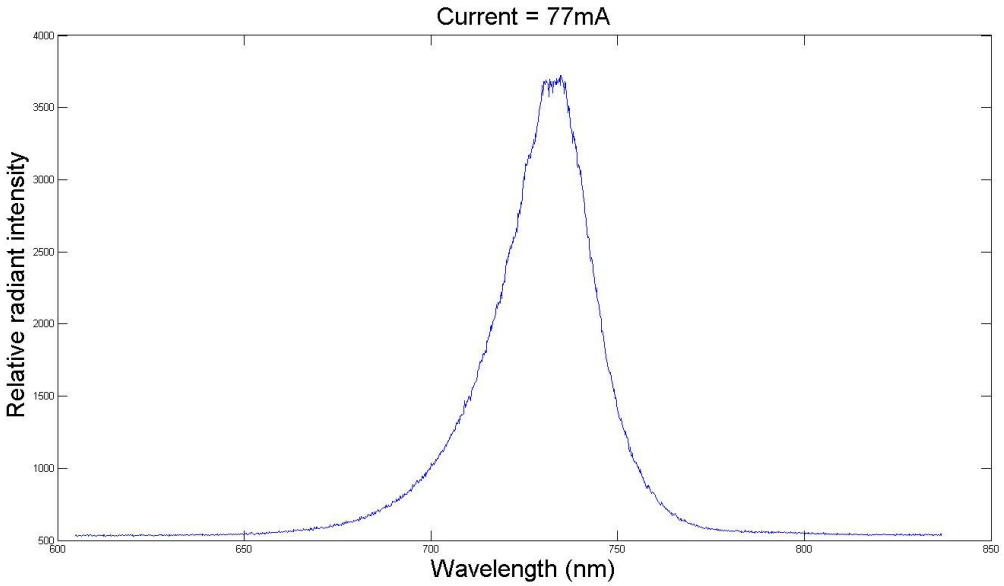
Current = 77mA
Relative radiant intensity
Wavelength (nm)
4000
3500
3000
2500
2000
1500
1000
500
600
650
700
750
800
850

Graphs of 810nm LED at different current settings: 75mA was considered the maximum and 56mA the operational current for safety as discussed in Chapter 5.

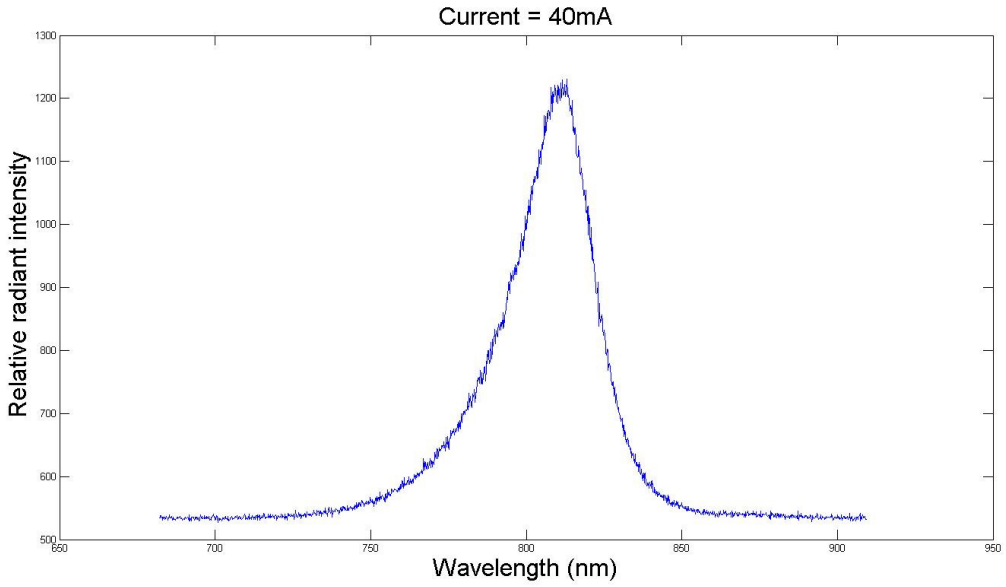

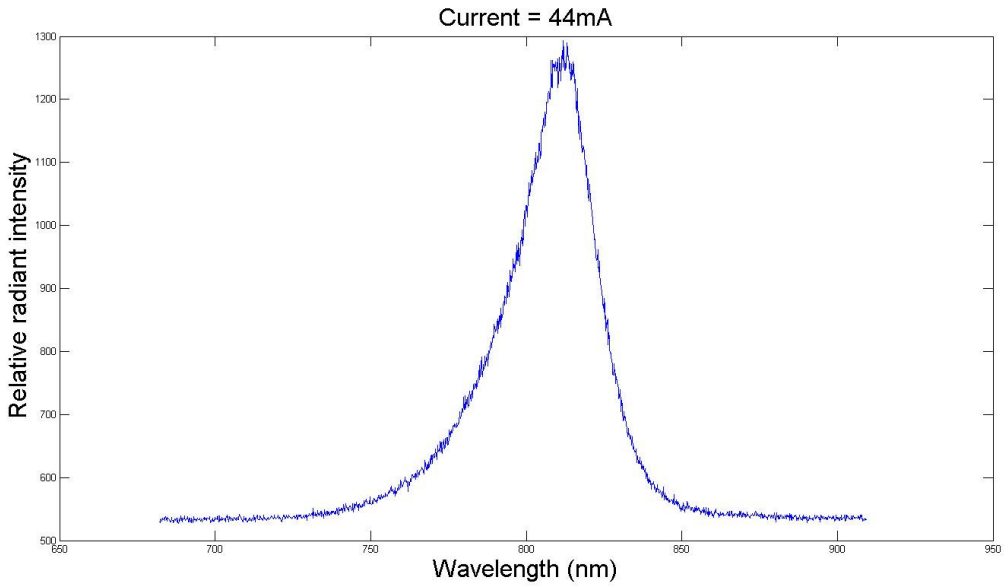

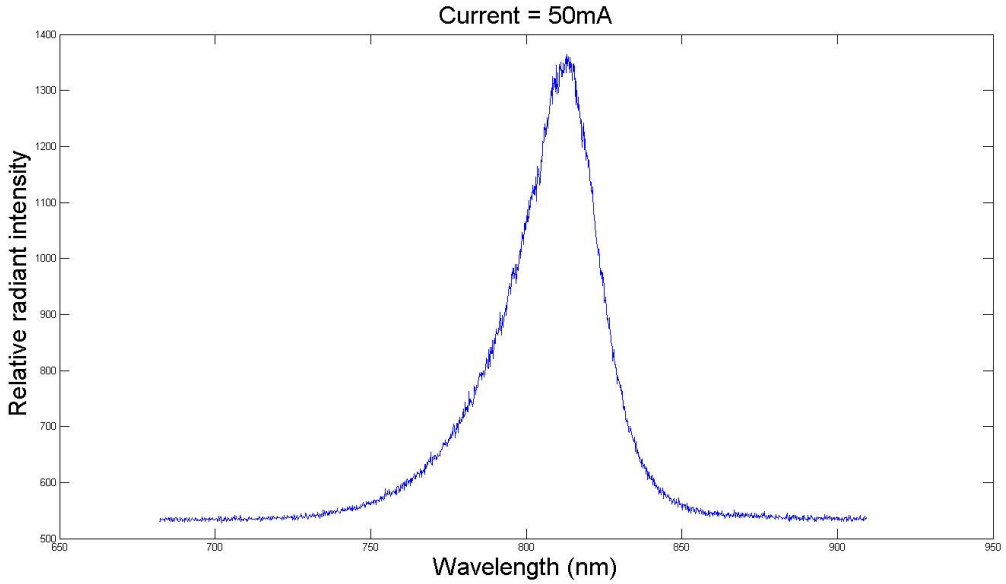
Current = 50mA
Relative radiant intensity
Wavelength (nm)
1400
1300
1200
1100
1000
900
800
700
600
500
650
700
750
800
850
900
950

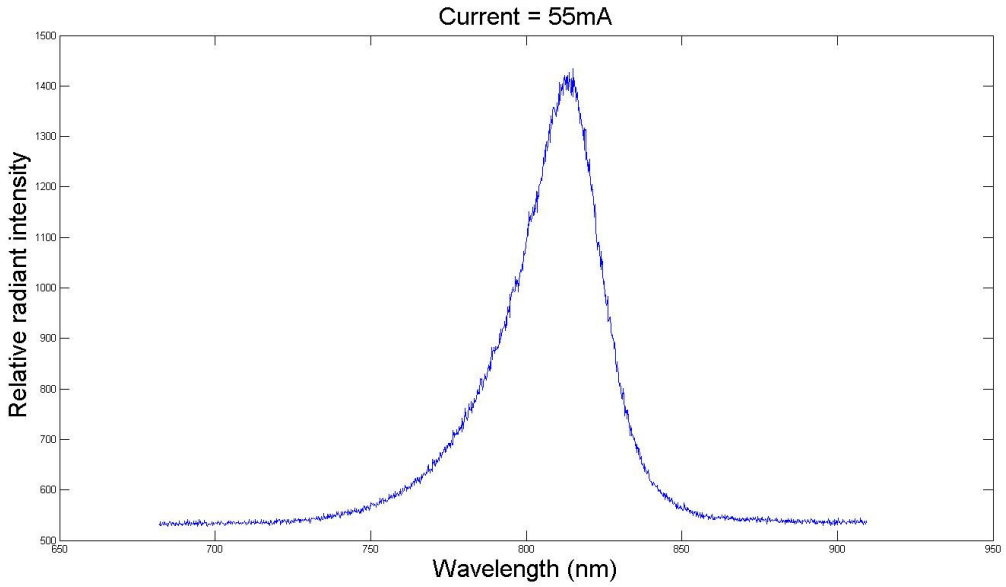
Current = 55mA
Relative radiant intensity
Wavelength (nm)
1500
1400
1300
1200
1100
1000
900
800
700
600
500
650
700
750
800
850
900
950

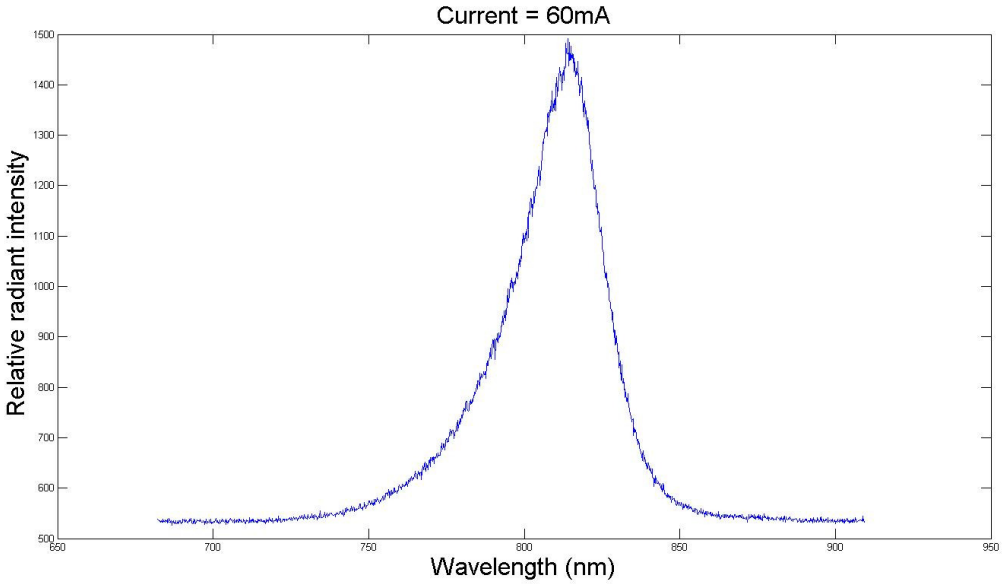
Current = 60mA
Relative radiant intensity
Wavelength (nm)
1500
1400
1300
1200
1100
1000
900
800
700
600
500
650
700
750
800
850
900
950

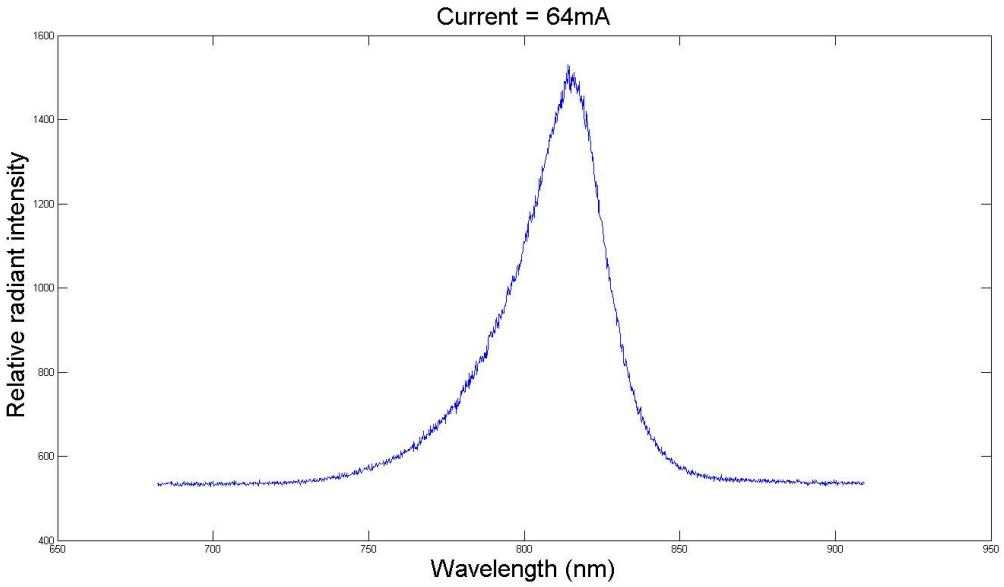
Current = 64mA
Relative radiant intensity
Wavelength (nm)
1600
1400
1200
1000
800
600
400
650
700
750
800
850
900
950

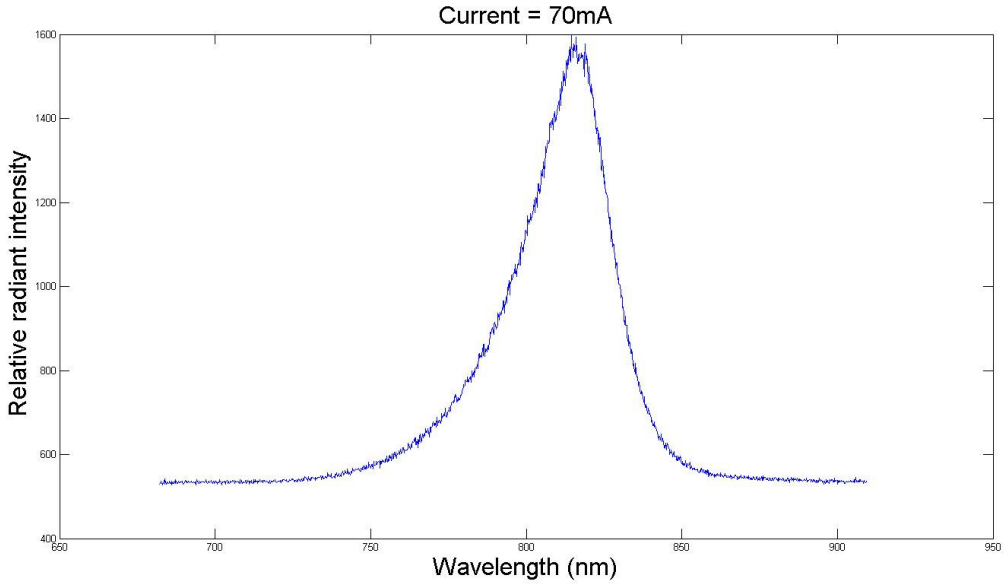
Current = 70mA
Relative radiant intensity
Wavelength (nm)
1600
1400
1200
1000
800
600
400
650
700
750
800
850
900
950

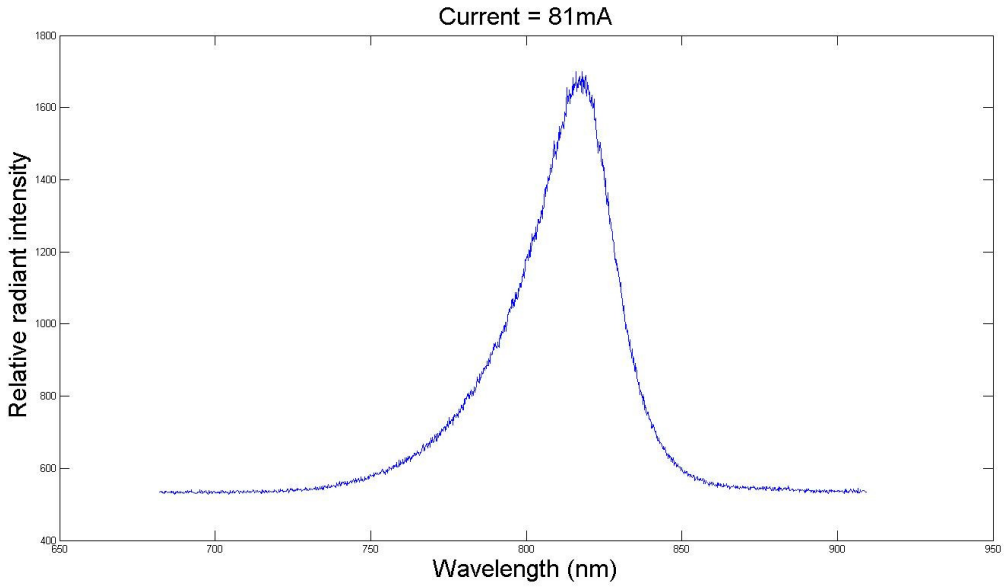
Current = 81mA
Relative radiant intensity
Wavelength (nm)
1800
1600
1400
1200
1000
800
600
400
650
700
750
800
850
900
950

Chapter 4: Feasibility testing the single-use SomaSensor for multiple-use in a clinical investigation

To successfully interface the SomaSensor (Covidien, USA) with the low-cost DAQ (presented in Chapter 2) for multiple-use in a low-resource clinical setting, tests were run with the help of Mr. Victor Vagne, Doctoral Student, at the research unit of Dr. Emmanuelle Le Bars and Dr. Nicolas Menjot de Champfleur, Plateforme d'Imagerie Fonctionnelle Humaine, Centre Hospitalier Régional Universitaire (CHRU) de Montpellier, France under CHRU Montpellier support.

4.1 Bench testing SomaSensors for reusability

Two SomaSensors were selected out of which one was unused and unopened before the start of this experiment. The second SomaSensor however had been used for more than 20 times. The radiant intensity and the peak wavelength of both the sensors were compared. The graphs of both the sensors are shown below. We used a spectrometer Princeton Instrument SP2150 with a CCD Princeton Instrument Pixis Excelon 400B. We also used a diffraction grating with 600 grooves/mm blazed at 500nm. The exposition time was set at 3µs. It was found that even after more than 20 times of use, the SomaSensor provided consistent performance when compared to a new SomaSensor.

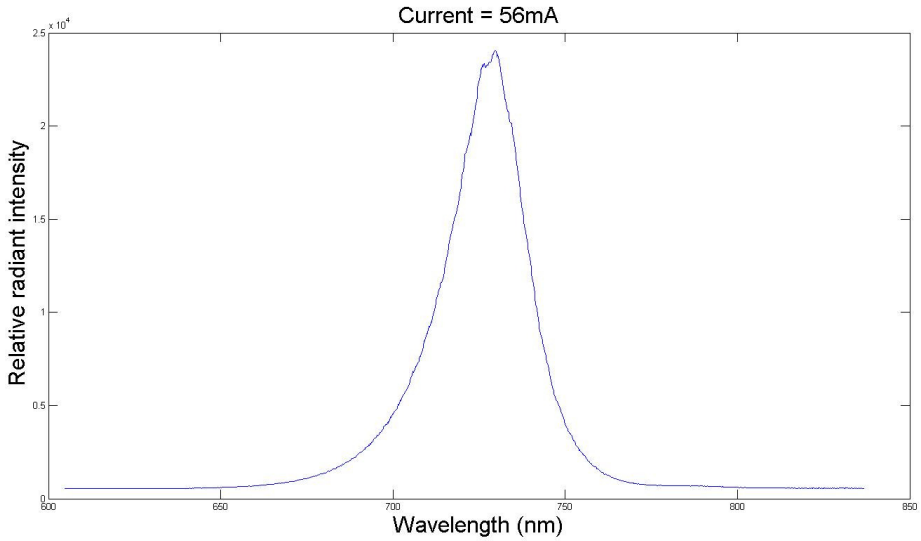

Fig 4.1. The relative radiant intensity of the used 730nm LED at 56mA current

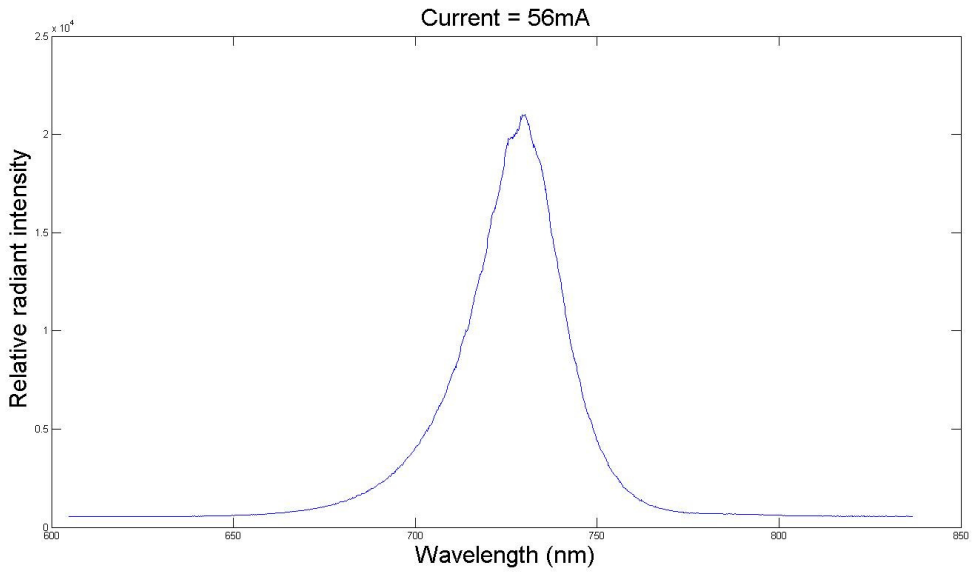

Fig 4.2. The relative radiant intensity of the unused 730nm LED at 56mA current

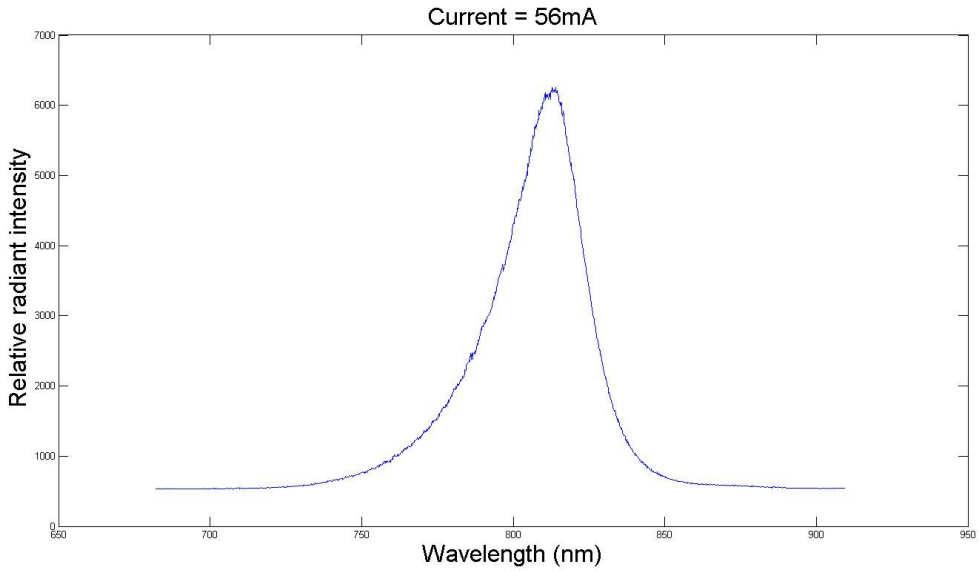

Fig 4.3. The relative radiant intensity of the used 810nm LED at 56mA current

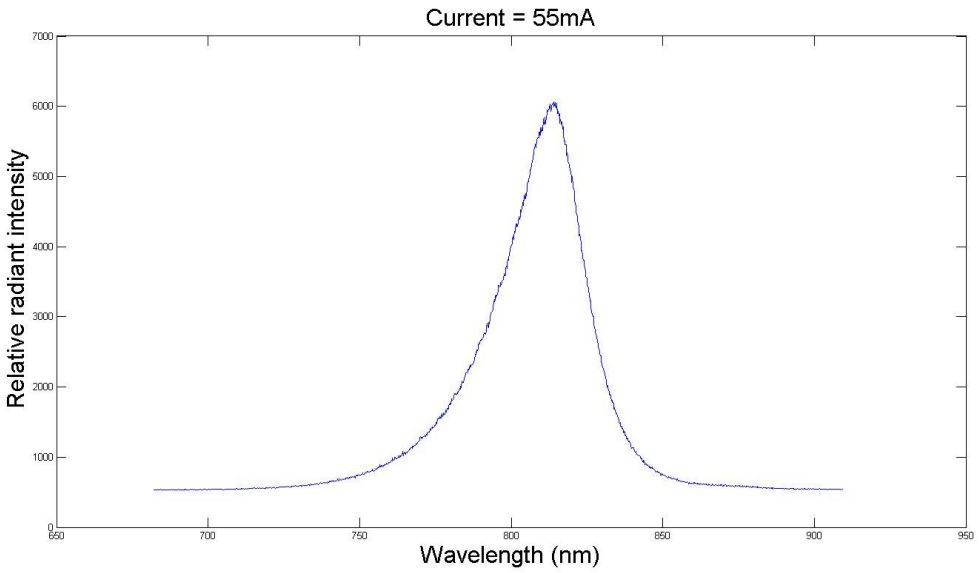

Fig 4.4. The relative radiant intensity of the unused 810nm LED at 56mA current

4.2 Human testing of SomaSensor interfaced with low-cost DAQ

To successfully interface the SomaSensor (Covidien, USA) with the low-cost DAQ (presented in Chapter 2), human testing of the Somasensors interfaced with the low-cost DAQ was required. The following tests were performed:

1. Testing of SomaSensors: The protocol followed for data collection was 1 minute of Pre-tDCS, 1 minute during tDCS and 1 min post-tDCS. 1.5mA current was maintained during tDCS. This was done on 1 subject and done for a total of 3 times. The data showed a slight change in oxygen saturation after ensemble averaging. We need to collect more trials (>=15) to find significant changes.

2. Testing of low-cost custom-made NIRS sensors: The protocol followed for data collection was 1 minute of Pre-tDCS, 1 minute during tDCS and 1 min post-tDCS. 1.5mA current was maintained during tDCS. This was done on 1 subject and done for a total of 4 times. The data showed very small change in oxygen saturation after ensemble averaging. We need to collect more trials (>=15) to find significant changes.

3. Testing of Somasensors with the INVOS 5100 oximeter: This was done with 2 subjects. We saw slight change in oxygen saturation on the monitor during the experiment. However, we need the serial port data transfer function for collecting data for analysis in the PC.

4.3 Performance testing of SomaSensor interfaced with low-cost DAQ using phantom

These tests were run with the help of Ms. Almajidy, Research Associate with Prof. Dr. rer.nat. Ulrich G. Hofmann, Peter-Osypka-Professor for Neuroelectronic Systems, University Medical Center Freiburg, Department of Neurosurgery, Germany.

For this experiment, 1400mL human blood phantom was prepared. Out of this 1400mL, 28mL was human blood and 14mL was intralipid. It is important to mention here that the blood was donated by a volunteer on the day 1 of the experiment and a part of the same blood sample was used on the day 2 of the experiment. The phantom setup was a dual layer dynamic phantom and the separation between each layer was 1.4cm which has been published by Ms. Almajidy [11]. This separation also included the thickness of the beaker. Figure 4.5 shows the phantom as it is prepared. Both the layers and the separation between them is clearly visible in this figure. The experiments were carried out in a dark room. Figure 4.6 and figure 4.7 show the phantom placed inside a black box which helped in eliminating external light exposure. A magnetic stirrer was used to keep the composition of the phantom uniform. The RPM of the stirrer was maintained at 500. Figure 4.6 shows the stirrer on which the phantom has been placed. For the first 35 minutes, nitrogen was flushed in the phantom to completely remove the oxygen from the phantom. This was followed by bubbling in oxygen at a constant rate for the next 10 minutes. NIRS readings were recorded for the entire duration of the experiments. Figure 4.8 shows the complete setup including the phantom and the NIRS device along with data acquisition laptop. The graphs for oxygen saturation obtained after analysis of NIRS data are also shown below.

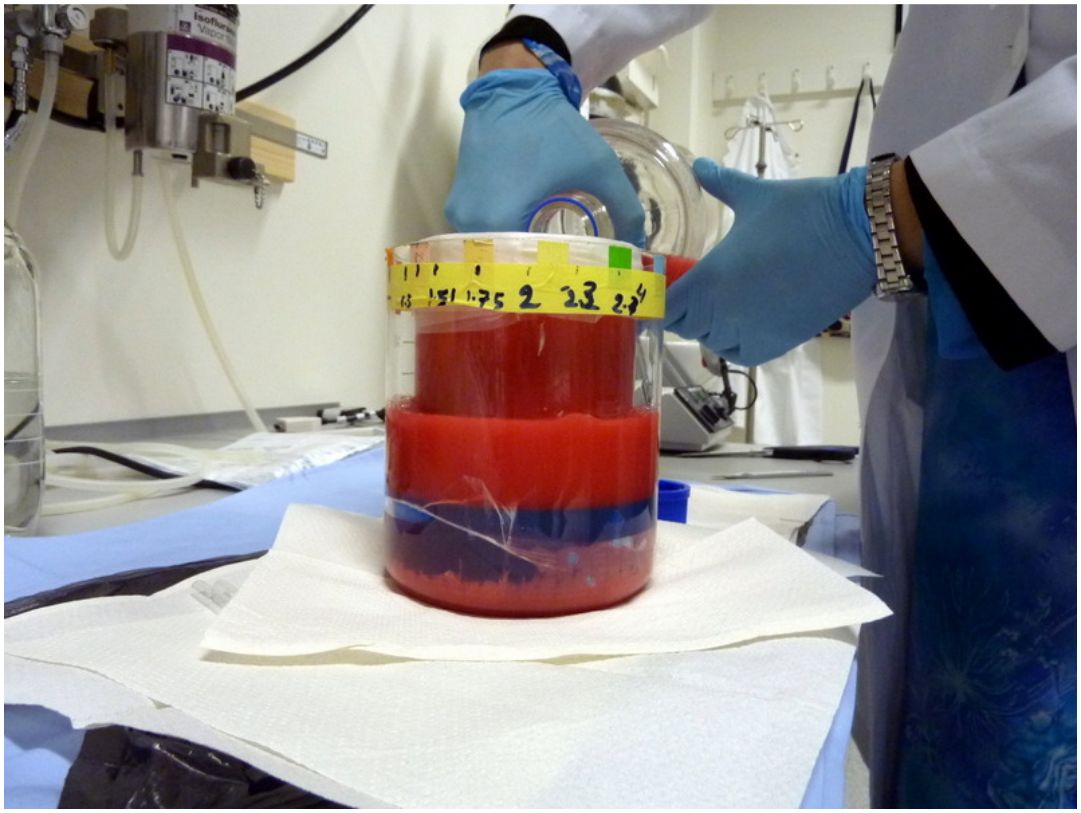

Fig 4.5. Phantom preparation

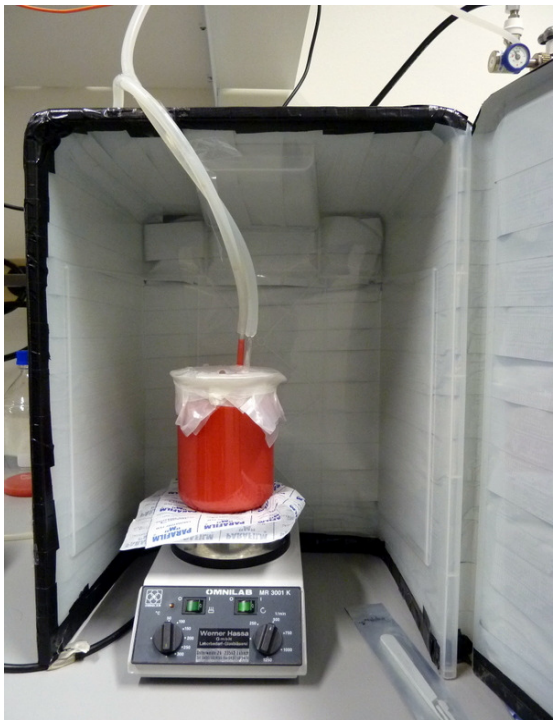

Fig 4.6. Phantom placed on the stirer

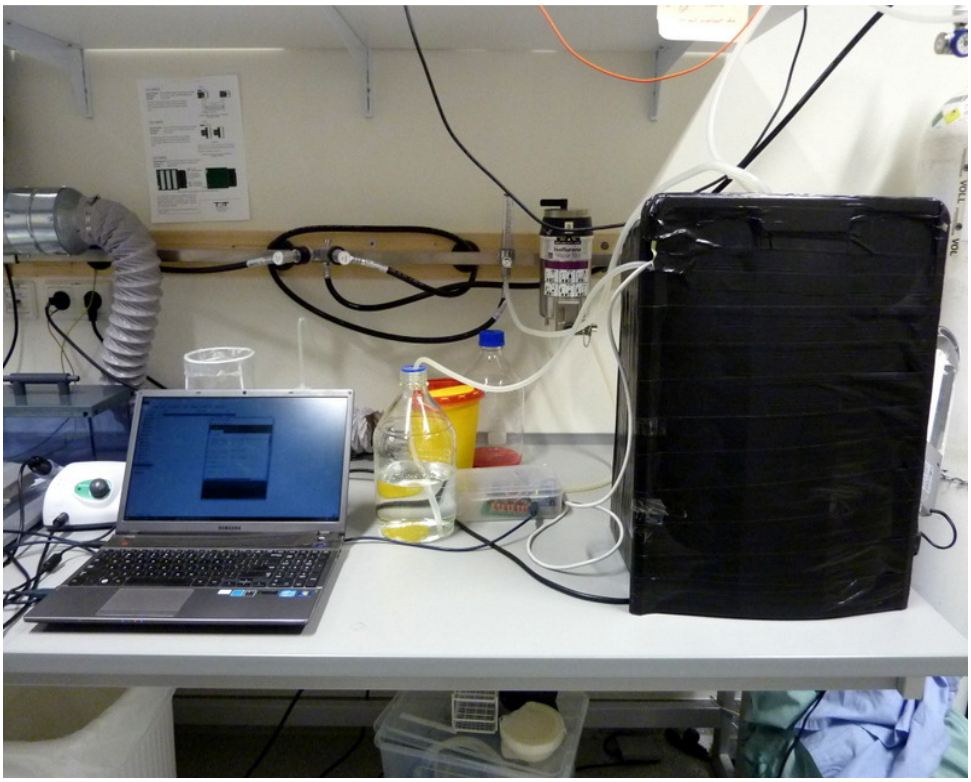

Fig 4.7. Phantom placed inside a dark box to reduce external light exposure

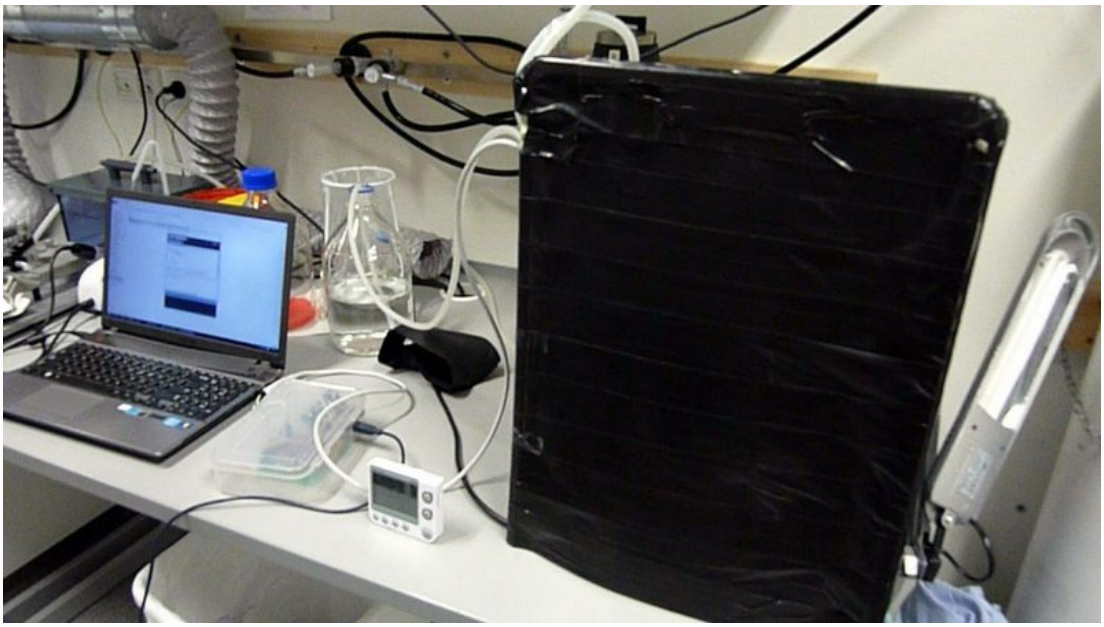

Fig 4.8. The complete experimental setup

The first day of the experiment showed results where the SomaSensor detected the changes in the oxygen saturation in the phantom as shown in Figures 4.9-4.11.

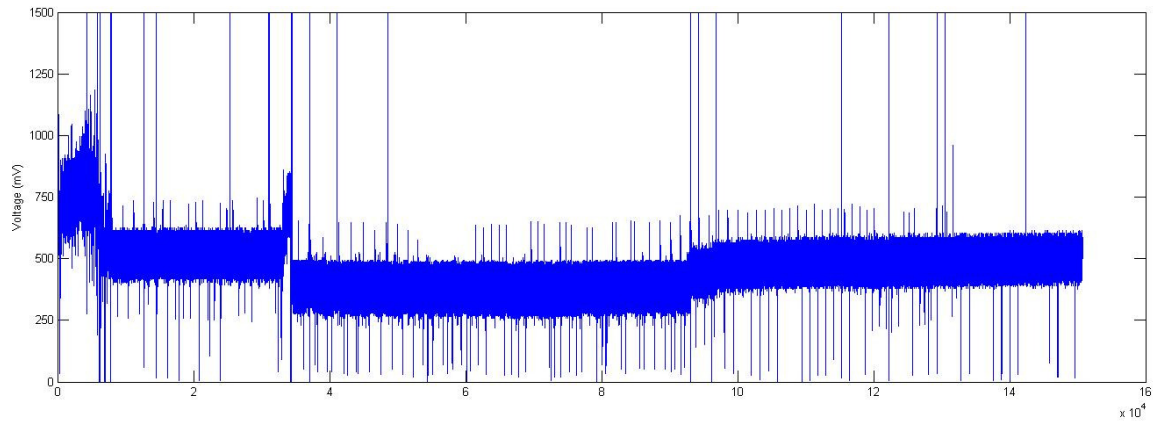

Fig 4.9. First trial of the first day of phantom testing: The initial period (first 25 mins) is when the nitrogen is pumped in the phantom to reduce oxygen saturation and the last part (~15 mins) is when the oxygen is pumped in the phantom (~10 mins) to increase oxygen saturation and then the oxygen saturation was maintained for another 5mins.

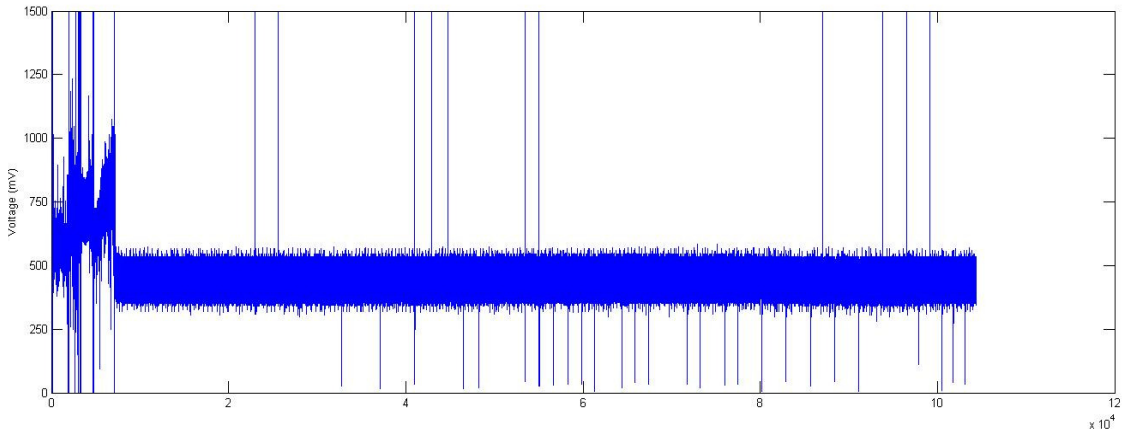

Fig 4.10. Second trial of the first day of phantom testing: The initial period (first 25 mins) is when the nitrogen is pumped in the phantom to reduce oxygen saturation and the last part (~15 mins) is when the oxygen is pumped in the phantom (~10 mins) to increase oxygen saturation and then the oxygen saturation was maintained for another 5mins. This trial terminated early due to a software glitch.

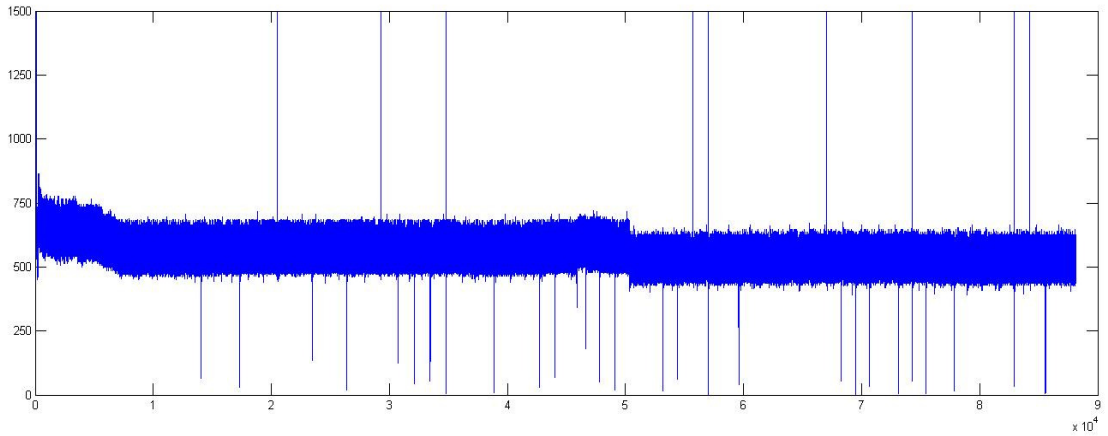

Fig 4.11. Third trial of the first day of phantom testing: The initial period (first 25 mins) is when the nitrogen is pumped in the phantom to reduce oxygen saturation and the last part (~15 mins) is when the oxygen is pumped in the phantom (~10 mins) to increase oxygen saturation and then the oxygen saturation was maintained for another 5mins. This trial terminated early due to a software glitch.

The second day of the experiment showed no results where the SomaSensor could not detect the changes in the oxygen saturation in the phantom as shown in Figures 4.12-4.14. We postulate that this was due to deterioration of the phantom as well as low SNR of the SomaSensor interfaced with the low-cost DAQ. The details are discussed in the next chapter that lends to my future work.

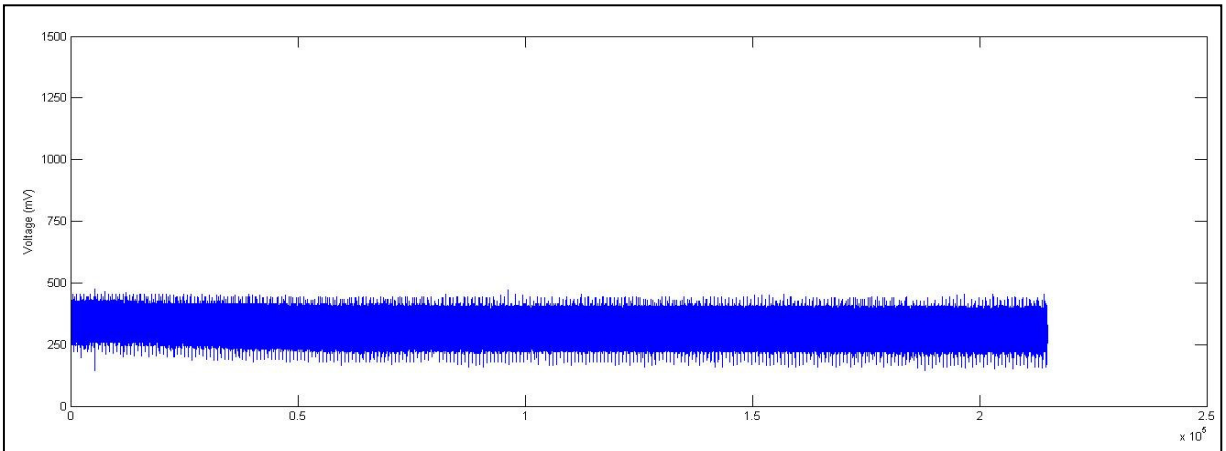

Fig 4.12. First trial of the second day of phantom testing: The initial period (first 25 mins) is when the nitrogen is pumped in the phantom to reduce oxygen saturation and the last part (~15 mins) is when the oxygen is pumped in the phantom (~10 mins) to increase oxygen saturation and then the oxygen saturation was maintained for another 5mins. The phantom seems to have deteriorated so much that the SomaSensor could not detect the change in the oxygen saturation.

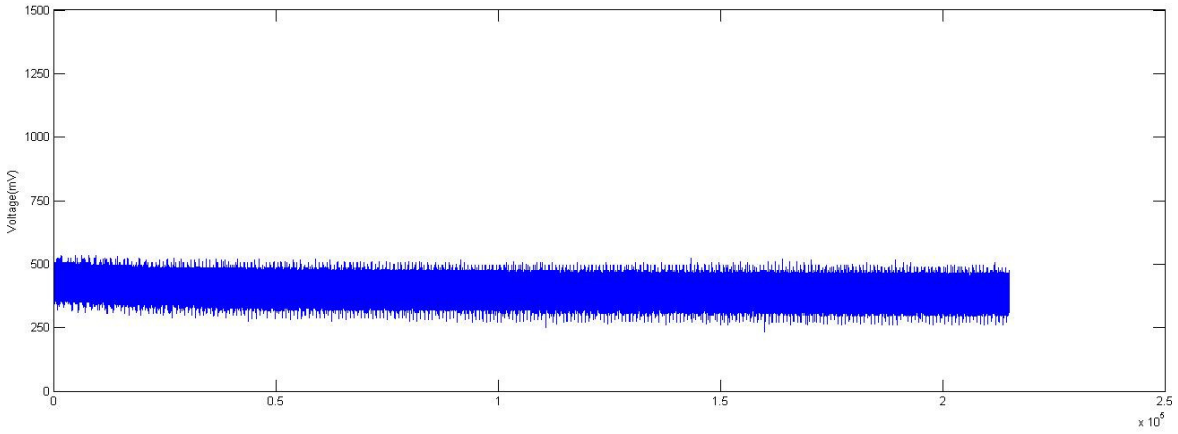

Fig 4.13. Second trial of the second day of phantom testing: The initial period (first 25 mins) is when the nitrogen is pumped in the phantom to reduce oxygen saturation and the last part (~15 mins) is when the oxygen is pumped in the phantom (~10 mins) to increase oxygen saturation and then the oxygen saturation was maintained for another 5mins. The phantom seems to have deteriorated so much that the SomaSensor could not detect the change in the oxygen saturation.

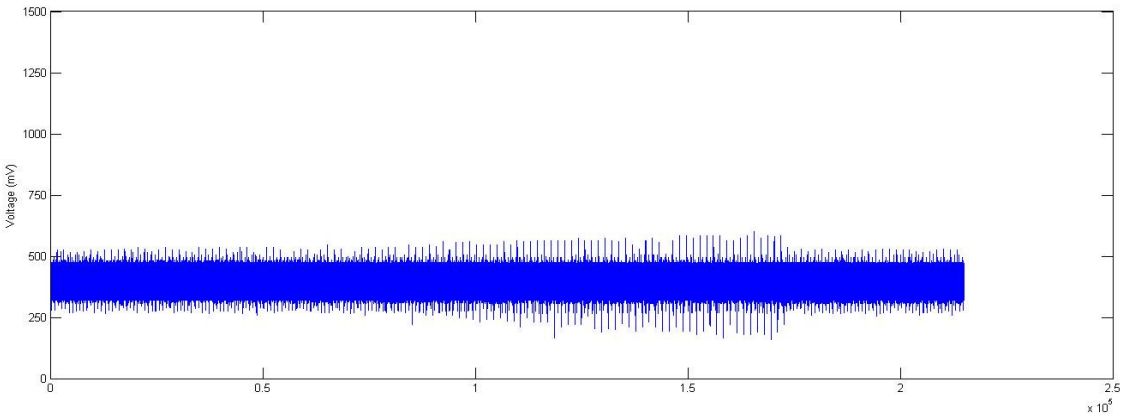

Fig 4.14. Third trial of the second day of phantom testing: The initial period (first 25 mins) is when the nitrogen is pumped in the phantom to reduce oxygen saturation and the last part (~15 mins) is when the oxygen is pumped in the phantom (~10 mins) to increase oxygen saturation and then the oxygen saturation was maintained for another 5mins. The phantom seems to have deteriorated so much that the SomaSensor could not detect the change in the oxygen saturation.

Chapter 5: Discussion and Future work

The low-cost CW NIRS system presented in this report costs roughly $500 [12]. The significant contribution of this INRIA internship work based on that low-cost CW NIRS system were,

1. Experiment done to evaluate the optimum current setting of the SomaSensor: The experiment was successful and the optimum current was found out to be 56 mA. Beyond this limit the supplied current resulted in increasing the temperature of the sensor which will damage the sensor over time and will also result in a burn if the sensor is used on a subject.

2. Experiment done to evaluate the reusability of the SomaSensor: The experiment was successful. The radiant intensity curves of both the LED's in both the SomaSensors were studied. The curves for both the new and the used SomaSensor were similar. This led to the conclusion that the SomaSensors can be reused up to 20 times at least.

3. Experiment done to test the somasensor interfaced with DAQ on a phantom: The experiments conducted on day 1 showed the variation in the oxygen saturation to some extend could be captured with the SomaSensor interfaced with low-cost DAQ but the experiments conducted on the day 2 showed no variation in the oxygen saturation levels that could be captured with the SomaSensor interfaced with low-cost DAQ. It is important to mention that all the settings and the protocol was identical on both the days of the experiment. This indicated that the device is not sensitive enough to detect the changes in blood phantom that was more than a day old. Also, the readings obtained on day 1 indicate a very low signal to noise ratio which was due to the low-cost DAQ.

The future work for the current low-cost DAQ hardware to work better with the SomaSensor are,

1. The present device is equipped with a 10 bit ADC which is the bare minimum in biomedical applications. This needs to be changed and an ADC with a higher resolution needs to be used to offer a better acquisition of the NIRS signal. One of the alternative ADC's that can be used comes from Texas Instruments AD129x family. These devices are low-power, multichannel, simultaneous-sampling, 24-bit delta-sigma (ΔΣ) analog-to-digital converters (ADC's) with integrated programmable gain amplifiers (PGAs). These devices incorporate various ECG-specific functions that make them well-suited for scalable electrocardiogram (ECG), electroencephalography (EEG), and electromyography (EMG) applications. Due to their high performance, these devices can be used in multichannel data acquisition systems by powering down the EEG-specific circuitry. Additionally, these devices offer a highly programmable mux which allows any of the input electrodes to be programmed as the patient reference drive. The PGA gain can be chosen from one of seven settings: 1, 2, 3, 4, 6, 8, or 12. The ADCs in the device offer data rates from 250 SPS to 32 kSPS. These devices can be communicated by using an SPI-compatible interface. Additionally, the ADS129xR also provide options for an internal respiration modulator and a demodulator circuit in the signal path of channel 1 [Texas Instruments: ADS129x Low-Power, 8-Channel, 24-Bit Analog Front-End for

Biopotential Measurements]. Therefore, the future work involved replacing the 10 bit ADC of Arduino microcontroller with the 24 bit AD129x. With this, the communication protocol needs to be modified for serially porting the values to the computer. With 10 bit ADC the I2C communication protocol was used. But, the 24 bit AD129 chip comes with only SPI communication protocol. Serial Peripheral Interface (SPI) is an interface bus commonly used to send data between microcontrollers and small peripherals such as shift registers, sensors, and SD cards. It uses separate clock and data lines, along with a select line to choose the device you wish to talk to. It's a "synchronous" data bus, which means that it uses separate lines for data and a "clock" that keeps both sides in perfect sync. For synchronization, there is an extra start bit and stop bit to help the receiver sync up to data as it arrives. So, the digital output from the AD129 will be sent to Arduino programmed with SPI communication, as shown in Fig. 5.1.

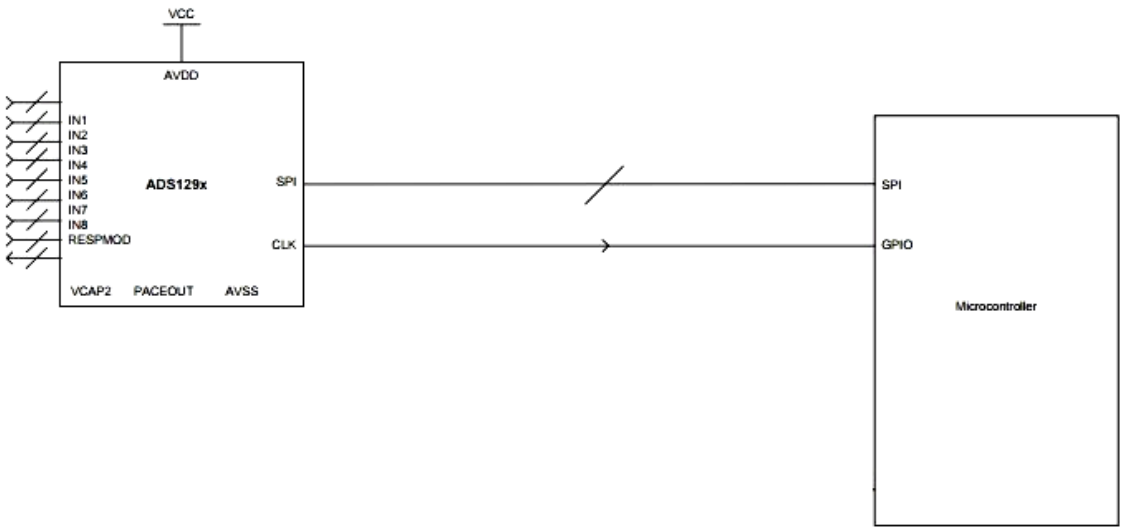

Fig 5.1. AD129x connected with a Microcontroller

With Arduino, there are two ways to communicate with SPI devices: By using the shiftIn() and shiftOut() commands. These are software-based commands that will work on any group of pins, but will be somewhat slow. Also, by using the SPI Library, which takes advantage of the SPI hardware built into the microcontroller. This is vastly faster than the above commands, but it will only work on certain pins. For Interfacing the Arduino with AD129, the various setting that needs to be done are as follows:

The interface can send data with the most-significant bit (MSB) first, or least-significant bit (LSB) first. In the Arduino SPI library, this is controlled by the setBitOrder() function. The slave will read the data on either the rising edge or the falling edge of the clock pulse. Additionally, the clock can be considered "idle" when it is high or low. In the Arduino SPI library, both of these options are controlled by the setDataMode() function. SPI can operate at extremely high speeds (millions of bytes per second), which may be too fast for some devices. To accommodate such devices, one can adjust the data rate. In

the Arduino SPI library, the speed is set by the setClockDivider() function, which divides the master clock (16MHz on most arduinos) down to a frequency between 8MHz (/2) and 125kHz (/128). From arduino, the digital output will be transferred to computer with a USB cable.

2. Quantitative EEG analysis has been used as a method of identifying subclinical brain injury during neurosurgical procedures, such as carotid endarterectomy, and for ischemia detection, global function assessment, medication titration, and prognostication [13]. Furthermore, high multilevel reproducibility has been shown [14] where EEG parameters reliably discriminated between stroke and transient ischaemic attack (TIA) patients or control subjects, and correlated significantly with clinical and radiological status. Reliable EEG parameters can be evaluated in a general stroke population for clinically relevant state and outcome measures [13]. There are several studies that investigated the relationship between EEG alpha rhythm variations (alpha rhythm lies in the range of 8 to 13 Hz) and baseline regional CBF differences [15] where the hemodynamic responses associated with cortical neural activity, i.e., the relationship between local neural activity and cerebral blood flow is termed neurovascular coupling (NVC) [16]. Therefore, EEG may provide a measure that is independent from fNIRS where EEG can be used to indirectly detect and monitor CBF. Here, simultaneous EEG-NIRS imaging during perturbation with tDCS may help us in understanding the NVC underlying neural and hemodynamic responses post-stroke [17]. Furthermore, EEG-NIRS joint imaging may improve the specificity by estimating NVC as a biomarker for post-stroke impaired cerebral microvessels functionality [17] where non-neuronal systemic physiological fluctuations often contaminate fNIRS signals [18]. Therefore it is important to develop and integrate an EEG hardware with the NIRS hardware so that the joint neuroimaging technology can be leveraged to objectively detect and monitor the brain status.

3. For multi-channel approaches required for whole head measurements, a custom-made CW NIRS system based on an off-the-shelf data acquisition (DAQ) device to interface between signal and computer provides the user with a robust, fast and flexible solution [19]. A multifunction off-the-shelf DAQ device (National Instruments Corporation, USA) can be used to provide basic physical input/output channels to drive the light sources and/or acquire optical signals. If timing accuracy of DAQ is critical, then a real-time off-the-shelf DAQ system, such as CompactRIO or PXI (National Instruments Corporation, USA), is required. Usually, the number of analog output channels are limited in off-the-shelf DAQ devices (e.g., only 2 analog outputs in PCIe-6351 from National Instruments Corporation, USA) and therefore the time division multiplexing technique can be used to illuminate multiple light sources (light emitting diodes or laser diodes). For example, the NIR light sources can be amplitude-modulated at different carrier frequencies with a gap (viz. 2 to 4 KHz in steps of 200Hz) using a driving circuit that includes a multiplexer and driver for the laser diode (LD) or light emitting diode (LED) to emit NIR light in consecutive time slots. LED, which emits incoherent and uncollimated light, is preferred since it allows the emission of more NIR photons into the tissue than LD with the same maximum permissible exposure [19]. Dual-wavelength LEDs can be used instead of two separate LEDs in a multi-channel high density whole head system. Moreover, an individual programmable current source for each LED can be

used so that the emitted light can be automatically adapted to variable individual acquisition conditions (hair, skin color, different tissue types such as muscle, brain etc. as well as a possible effect of EEG gel on the optical properties of the light path) [20]. Then, the backscattered NIR light can be collected (collected light is usually 7 to 9 orders smaller in magnitude than that emitted at the source [21]) and converted into an electrical signal by photodiodes. Due to low signal to noise ratio (SNR) of the output signal from the photodiodes, the signal can be band-pass filtered and amplified to increase the SNR. A programmable gain amplifier (e.g. PGA204, Texas Instruments Inc., USA) can be used to adapt the gain depending on source-detector distance, scalp thickness, and hair color and density [22] to match the voltage range of the analog input channel of the DAQ device.

References

[1] F. F. Jöbsis, "Noninvasive, infrared monitoring of cerebral and myocardial oxygen sufficiency and circulatory parameters," *Science*, vol. 198, no. 4323, pp. 1264–1267, Dec. 1977.

[2] M. Cope and D. T. Delpy, "System for long-term measurement of cerebral blood and tissue oxygenation on newborn infants by near infra-red transillumination," *Med. Biol. Eng. Comput.*, vol. 26, no. 3, pp. 289–294, May 1988.

[3] S. Lloyd-Fox, A. Blasi, and C. E. Elwell, "Illuminating the developing brain: the past, present and future of functional near infrared spectroscopy," *Neurosci. Biobehav. Rev.*, vol. 34, no. 3, pp. 269–284, Mar. 2010.

[4] A. Pellicer and M. del C. Bravo, "Near-infrared spectroscopy: a methodology-focused review," *Semin. Fetal. Neonatal Med.*, vol. 16, no. 1, pp. 42–49, Feb. 2011.

[5] M. U. Tsao, S. S. Sethna, C. H. Sloan, and L. J. Wyngarden, "Spectrophotometric determination of the oxygen saturation of whole blood," *J. Biol. Chem.*, vol. 217, no. 1, pp. 479–488, Nov. 1955.

[6] D. T. Delpy, M. Cope, P. van der Zee, S. Arridge, S. Wray, and J. Wyatt, "Estimation of optical pathlength through tissue from direct time of flight measurement," *Phys. Med. Biol.*, vol. 33, no. 12, pp. 1433–1442, Dec. 1988.

[7] M. Hiraoka, M. Firbank, M. Essenpreis, M. Cope, S. R. Arridge, P. van der Zee, and D. T. Delpy, "A Monte Carlo investigation of optical pathlength in inhomogeneous tissue and its application to near-infrared spectroscopy," *Phys. Med. Biol.*, vol. 38, no. 12, pp. 1859–1876, Dec. 1993.

[8] G. Strangman, D. A. Boas, and J. P. Sutton, "Non-invasive neuroimaging using near-infrared light," *Biol. Psychiatry*, vol. 52, no. 7, pp. 679–693, Oct. 2002.

[9] S. J. Matcher and C. E. Cooper, "Absolute quantification of deoxyhaemoglobin concentration in tissue near infrared spectroscopy," *Phys. Med. Biol.*, vol. 39, no. 8, pp. 1295–1312, Aug. 1994.

[10] J. B. Fishkin, O. Coquoz, E. R. Anderson, M. Brenner, and B. J. Tromberg, "Frequency-domain photon migration measurements of normal and malignant tissue optical properties in a human subject," *Appl. Opt.*, vol. 36, no. 1, pp. 10–20, Jan. 1997.

[11] R. K. Almajidy, R. D. Kirch, O. Christ, and U. G. Hofmann, "Estimating the spatial resolution of fNIRS sensors for BCI purposes," 2014, p. 894504.

[12] U. J. Mehak Sood, "Continuous wave functional near infra-red spectroscopy combined with transcranial direct current stimulation for assessment of cerebral vascular status in patients with ischemic stroke," 2014.

[13] B. Foreman and J. Claassen, "Quantitative EEG for the detection of brain ischemia," *Crit.*

Care, vol. 16, no. 2, p. 216, Mar. 2012.

[14] R. V. A. Sheorajpanday, G. Nagels, A. J. T. M. Weeren, M. J. A. M. van Putten, and P. P. De Deyn, "Reproducibility and clinical relevance of quantitative EEG parameters in cerebral ischemia: a basic approach," *Clin. Neurophysiol. Off. J. Int. Fed. Clin. Neurophysiol.*, vol. 120, no. 5, pp. 845–855, May 2009.

[15] K. Jann, T. Koenig, T. Dierks, C. Boesch, and A. Federspiel, "Association of individual resting state EEG alpha frequency and cerebral blood flow," *NeuroImage*, vol. 51, no. 1, pp. 365–372, May 2010.

[16] J. A. Filosa, "Vascular tone and neurovascular coupling: considerations toward an improved in vitro model," *Front. Neuroenergetics*, vol. 2, 2010.

[17] A. Dutta, "EEG-NIRS based low-cost screening and monitoring of cerebral microvessels functionality," 2014.

[18] U. J. Mehak Sood, "Anterior temporal artery tap to identify systemic interference using short-separation NIRS measurements: a NIRS/EEG-tDCS study," 2015.

[19] C. Soraghan, F. Matthews, C. Markham, B. A. Pearlmutter, R. O'Neill, and T. E. Ward, "A 12-channel, real-time near-infrared spectroscopy instrument for brain-computer interface applications," *Conf. Proc. Annu. Int. Conf. IEEE Eng. Med. Biol. Soc. IEEE Eng. Med. Biol. Soc. Annu. Conf.*, vol. 2008, pp. 5648–5651, 2008.

[20] J. Safaie, R. Grebe, H. A. Moghaddam, and F. Wallois, "Wireless distributed acquisition system for near infrared spectroscopy – wda-nirs," *J. Innov. Opt. Health Sci.*, vol. 06, no. 03, p. 1350019, May 2013.

[21] E. Lareau, G. Simard, F. Lesage, D. Nguyen, and M. Sawan, "Near infrared spectrometer combined with multichannel EEG for functional brain imaging," in *2011 5th International Symposium on Medical Information Communication Technology (ISMICT)*, 2011, pp. 122–126.

[22] F. Scholkmann, S. Kleiser, A. J. Metz, R. Zimmermann, J. Mata Pavia, U. Wolf, and M. Wolf, "A review on continuous wave functional near-infrared spectroscopy and imaging instrumentation and methodology," *NeuroImage*, vol. 85 Pt 1, pp. 6–27, Jan. 2014.